

# Modification of Several Residual Biomasses with $\text{Al}_2\text{O}_3$ Nanoparticles and its Effect on Cr (VI) and Hg (II) Adsorption Kinetics

A. Herrera-Barros<sup>1</sup>, C. Tejada-Tovar<sup>2</sup>, A. Villabona-Ortiz<sup>2</sup>, Á. D. González-Delgado<sup>1\*</sup> and Y. Villabona-Durán<sup>2</sup>

<sup>1</sup>Chemical Engineering Department, Nanomaterials and Computer Aided Process Engineering Research Group (NIPAC), University of Cartagena, Cartagena, Bolívar, Colombia; aherrerab@unicartagena.edu.co, agonzalezd1@unicartagena.edu.co

<sup>2</sup>Chemical Engineering Department, Process Design and Biomass Utilization Research Group (IDAB), University of Cartagena, Cartagena, Bolívar, Colombia; ctejadat@unicartagena.edu.co, avillabonao@unicartagena.edu.co, ypvillabonad@gmail.com

## Abstract

**Background:** The presence of toxic pollutants in water sources has become a major issue worldwide and different technologies have been applied for water treatment such as chemical precipitation, ionic interchange, adsorption, membrane filtration, flocculation, among others. In the last decades, nanotechnology has gain attention in the development of nanomaterials for removing these pollutants. **Objectives:** In this work, Hg (II) and Cr (II) adsorption process was studied using residual biomass (orange peels, corn cob and oil palm bagasse) modified with  $\text{Al}_2\text{O}_3$  nanoparticles. **Methods/Analysis:** The biomasses before and after modification were characterized by FT-IR analysis in order to determine main functional groups. In addition, XRD technique was used to calculate average crystallite size and identify both  $\gamma$  and  $\delta$  alumina. **Findings:** It was found that suitable conditions for further experiments were particle size of 0.355 mm and pH values of 2 and 6 for Cr (VI) and Hg (II), respectively. For Hg (II) ions, the highest removal yields were 70.89, 34.18 and 54.9 % using OPB- $\text{Al}_2\text{O}_3$ , CC- $\text{Al}_2\text{O}_3$  and OP- $\text{Al}_2\text{O}_3$ , respectively. For Cr (VI) ions, these values were 48.2, 39.8 and 30.5 % using OPB- $\text{Al}_2\text{O}_3$ , CC- $\text{Al}_2\text{O}_3$  and OP- $\text{Al}_2\text{O}_3$ , respectively. **Novelty/Improvement:** These results suggested that OPB- $\text{Al}_2\text{O}_3$  can be successfully used in removing Cr (VI) and Hg (II) with higher efficiency than the others synthesized biosorbents.

**Keywords:**  $\text{Al}_2\text{O}_3$  Nanoparticles, Biomass, Biosorption, Nanomaterials

## 1. Introduction

The rapidly expanding industrial and domestic activities have led an increase of pollutants in water sources<sup>1</sup>. These toxic contaminants are broadly classified into three main types-heavy metals, metalloids and pesticides<sup>2</sup>. Heavy metals are non-biodegradable and can accumulate in the environment and living organisms affecting the environment and health<sup>3</sup>. Mercury is one of the heavy metals most frequently found on industrial effluent becoming

a global environmental problem environment due to its persistence<sup>4,5</sup>. Chromium is considered as carcinogenic and is widely used in mining, leather tanning process, cement industries, electroplating, photographic material and corrosive paints<sup>6</sup>. A large number of methods have been studied in order to solve the problem of heavy metals release such as coagulation-flocculation, chemical precipitation, filtration, sedimentation and ion exchange<sup>7</sup> impregnating sequence and the gas composition have significant effect on the performance of the adsorbents.

\*Author for correspondence

Co-impregnation of Cu and Mn solutions is simple but also of help to improve the Hg pickup capacity, due to the synergic effect of the CuMn oxide, the sorbent prepared using incipient wetness method containing 20% CuO and 20% wt MnO<sub>2</sub> has Hg pick capacity of 12.0% wt. It is showed that the oxide form the adsorbent can reduce Hg from more than 11,600 ppb to 0.1 ppb in a single pass. The presence of H<sub>2</sub>S in the gas stream changes the Hg sorption mechanism and increase Hg pickup capacity. XRD and electron microscope characterization results of the fresh and spent sorbent show that the active phases of the sorbent are CuMn(OH). However, they are limited by high costs, inefficiency and generation of toxic sludge or other waste products<sup>3</sup>. Technologies such as bioadsorption have been recognized as a promising alternative for water treatment because of its advantages compared to other processes including local availability, cost-effectiveness of materials and reduced environmental effects<sup>8,9</sup>.

Recently, many studies are focused on removing contaminants such as Pb (II), Hg (II), Ni (II) and Cr (VI) using biomass from agricultural wastes. For example<sup>6</sup> evaluated the Cr (VI) removal yield using different biosorbents obtained from orange peel biomass. On the other hand, nanotechnology is a field that deals with modification, design and application of nanoscale objects, which have attracted global attention for the detection, degradation and removal of hazardous pollutants<sup>10,11</sup>. A wide variety of nanomaterials have been considered for heavy metals uptake based on magnetic nanoparticles of titanium dioxide, alumina, cerium oxide, ferric and zinc oxide modified with chelating functional groups<sup>12-15</sup>. This work attempts to study the removal of Cr (VI) and Hg (II) using biomaterials modified with Al<sub>2</sub>O<sub>3</sub> nanoparticles in order to determine the most efficient synthesized biosorbent and the suitable operation conditions (pH and particle size) for carrying out further adsorption experiments.

## 2. Material and Methods

### 2.1 Materials

Orange peels (*Citrus sinensis*), corn cob (*Zeamays*) and oil palm bagasse (*Elaeisguineensis*) were used as biomass to prepare biosorbents. Aluminum nitrate (Al(NO<sub>3</sub>)<sub>3</sub>·9H<sub>2</sub>O) and citric acid (C<sub>6</sub>H<sub>8</sub>O<sub>7</sub>) were used as starting material in nanoparticles synthesis. Dimethyl Sulfoxide (DMSO),

Tetra Ethyl-o-Silicate (TEOS) and ethanol (C<sub>2</sub>H<sub>5</sub>OH) were required for loading Al<sub>2</sub>O<sub>3</sub> nanoparticles into biomass.

### 2.2 Biosorbent Preparation

Biomaterials were cut off in small pieces, washed thoroughly to remove surface-adhered particles and dried during 24 hours at 80°C. Afterward, dried solids were grounded and sieve-meshed to obtain homogenous particle sizes<sup>16-18</sup>.

**Synthesis of nanoparticles:** Alumina nanoparticles were synthesized by sol-gel method, which is based on adding 0.5 moles of citric acid to the 0.5 M (Al(NO<sub>3</sub>)<sub>3</sub>·9H<sub>2</sub>O) solution and continuously stirring at 60°C until a yellow coloration was obtained. The resulting gel was dried at 200 °C in an oven for 2 hours and heat treated at 750°C for 2 hours<sup>19,20</sup>.

**Modification of biomaterials with Al<sub>2</sub>O<sub>3</sub> nanoparticles:** The loading procedure was carried out using dimethyl sulfoxide as follow: biomass (0.5 g) was added into DMSO for 24 hours under stirring. The resulting suspension was mixed with 3 mL of TEOS and stirred for 48 hours. The general method using TEOS to prepare the biosorbents was reported by<sup>21</sup>, in which TEOS molecules were hydrolyzed and condensed. After that, 0.3 g of Al<sub>2</sub>O<sub>3</sub> nanoparticles were added to biomass suspension. After stirring for 12 hours, the biosorbents were washed thoroughly with water and ethanol several times<sup>21,22</sup>.

### 2.3 Characterization Techniques

The biomasses (orange peels, corn cob and oil palm bagasse) and biosorbents were characterized by Fourier Transform Infrared Spectroscopy (FT-IR) in order to identify their functional groups. In addition, the crystalline structure of nanoparticles were observed by X-Ray Diffraction (XRD) technique.

### 2.4 Adsorption Experiments

The adsorption process of Cr (VI) and Mg (II) onto biosorbents overtime was studied by taking aliquots of 5 mL between 10-280 minutes. The remaining concentration of Hg (II) ions were determined by UV-Vis spectrometer using ammonium thiocyanate<sup>23</sup>. Hence, 1 mL of sample was added to 4 mL of 5% w/w NH<sub>4</sub> and diluted in deionized water<sup>24</sup>. For Cr (VI) ions, the remaining concentration was determined using diphenylcarbazide, which is based

on preparing a solution of 1,5-diphenylcarbazide in acetone and mixed with deionized water. Finally, phosphoric acid was added drop-wise as color indicator<sup>25</sup>.

### 3. Results and Discussion

#### 3.1 Characterization of Residual Biomass

Figure 1 shows adsorption spectrum of Orange Peels (OP), Corn Cob (CC) and Oil Palm Bagasse (OPB) biomasses, in which main functional groups are observed. The orange peels biomass exhibited absorption band around  $3330\text{ cm}^{-1}$  attributed to O-H stretching vibrations of alcohols, phenols and carboxylic acids in pectin, cellulose and lignin molecules. Hence, it was identified the presence of “free” hydroxyl groups on biosorbent surface as reported by<sup>26</sup>. The spectrum of corn cob biomass shows a wide band at  $1012$  and  $3405\text{ cm}^{-1}$  assigned to C-O stretching vibrations and H-bonding, respectively. In addition, the absorption peak around  $1600\text{ cm}^{-1}$  corresponded to vibrations of aromatic lignin content. As pointed out by<sup>27</sup>, the characteristic peaks of hemicellulose biomass were identified at  $1274$  and  $1238\text{ cm}^{-1}$ . It was found absorption bands at  $3500$  and  $3000\text{ cm}^{-1}$  in oil palm bagasse spectrum ascribed to the presence of carboxylic acids. The peaks at  $1600$  and  $1700\text{ cm}^{-1}$  corresponded to carbonyl group and aromatic C=H in lignin molecules. The vibrations around  $1450\text{-}1540\text{ cm}^{-1}$  can be assigned to aliphatic and aromatic groups and deformation of methyl, methylene and methoxy groups. The band located in absorption range  $1050\text{-}1450\text{ cm}^{-1}$  are associated to carboxylic acids and alcohols of hemicellulose<sup>17,18</sup>.

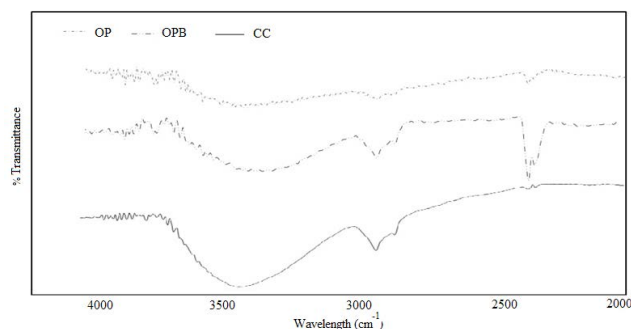


**Figure 1.** FT-IR spectra of orange peels (OP), corn cob (CC) and oil palm bagasse (OPB) biomass.

#### 3.2 Characterization of $\text{Al}_2\text{O}_3$ Nanoparticles

The XRD analysis was carried out in order to identify phases and microstructure of synthesized nanoparticles. As is shown in Figure 2, the broad peak at  $15\text{-}40^\circ$  ( $2\theta$ ) is attributed to crystalline nature of  $\text{Al}_2\text{O}_3$  nanoparticles. The full widths at half-maximum of the XRD lines at  $2\theta$  range was used to determine the average crystallite size using Scherrer's equation as follows<sup>20</sup>:

Where  $D$  is the average particle size,  $\lambda$  is the wavelength of X-ray radiation ( $1.45\text{ \AA}$ ) and  $s$  the line broadening at half the maximum intensity. The calculated value of average particle size was  $50 \pm 4\text{ nm}$  and the sharpest peak attributed to  $\gamma$ -alumina suggested an amorphous structure. It was also identified that  $\gamma$ -alumina coexists with  $\delta$ -alumina.

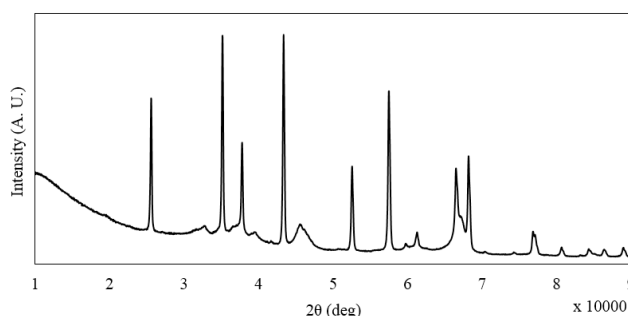


**Figure 2.** XRD pattern of  $\text{Al}_2\text{O}_3$  nanoparticles.

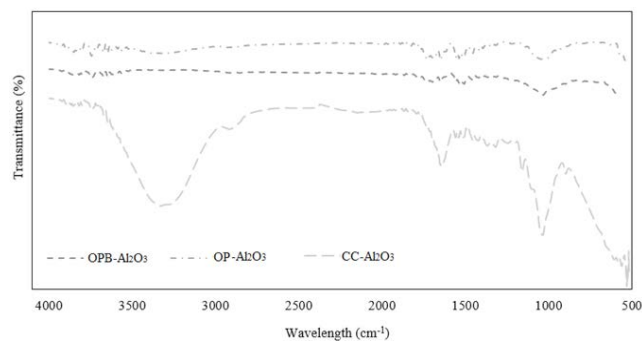
#### 3.3 Characterization of biosorbents

Figure 3 shows the results of FT-IR analysis performed to different biomasses modified with  $\text{Al}_2\text{O}_3$  nanoparticles. It was found that these biosorbents exhibited the same functional groups of unmodified biomaterials. The presence of aluminum bonds listed in Table 1 was expected due to the loading of biomass with alumina powder.

**Table 1.** Identification of functional groups with absorption bands

Functional groups	Absorption bands ( $\text{cm}^{-1}$ )
O-Al-O	650-700
Al - O - M*	950-1200
Al - C = O	1500-1700
Al - COOH	2600-3800

\*M=Al or Si



**Figure 3.** FT-IR spectra of biomaterials modified with Al<sub>2</sub>O<sub>3</sub> nanoparticles.

The absorption peaks at 600 and 800 cm<sup>-1</sup> are attributed to symmetric and asymmetric deformation vibrations of Al-O as a result of Al<sub>2</sub>O<sub>3</sub> nanoparticle complexity<sup>28</sup>. All spectrums showed a sharp band at 1600 cm<sup>-1</sup> assigned to Al-C=O bonding. In addition, the presence of characteristic peaks in the absorption range 900-1200 cm<sup>-1</sup> confirms that different types of functional groups are available on the surface of biosorbents for cationic exchange reactions related to the =Al-O groups according to that reported by<sup>29</sup>.

### 3.4 Adsorption Experiments

**Effect of pH and particle size:** The adsorption process takes place mainly on porous biosorbent surface and the amount of heavy metal ions adsorbed is proportional to the solution volume and surface area of adsorbent particles. In addition, the specific surface area is increased as the particle size becomes small due to the number of pores per unit mass<sup>30</sup>. In order to determine suitable conditions for further experiments, the effect of pH and particle size on Cr (VI) and Hg (II) uptake was evaluated. Different pH values (2, 4 and 6) and particle sizes (0.355, 0.5 and 1 mm) were considered. Figures 4, 5 and 6 show the removal yield of both heavy metal ions using biomaterials modified with Al<sub>2</sub>O<sub>3</sub> nanoparticles. It was observed that removal yield increased as particle size decreased for both Cr (VI) and Hg (II), which is ascribed to the improved surface area that increases the available sites for biosorbent-solute interactions. As adsorption is a surface phenomenon, it was expected that chromium and mercury uptake were proportional to available biosorbent surface<sup>31</sup>.

It is well known that pH plays an important role on adsorption capacity of biosorbents. In the range of pH 2-6, the predominant form of chromium is Cr<sub>2</sub>O<sub>7</sub><sup>2-</sup> and

HCrO<sub>4</sub><sup>-</sup>; at pH ~6, it is present in the form of CrO<sub>4</sub><sup>2-</sup> ions and the affinity of this anion is very low in comparison with Cr<sub>2</sub>O<sub>7</sub><sup>2-</sup> and HCrO<sub>4</sub><sup>-</sup>. In addition, the bioadsorbent surface is highly protonated due to the H<sup>+</sup> ions at lower pH and there is a strong electrostatic attraction between the positively charged surface and the anions Cr<sub>2</sub>O<sub>7</sub><sup>2-</sup> and HCrO<sub>4</sub><sup>-</sup> as pointed out by<sup>32</sup>. Hence, it was expected that removal yield decreased as pH increased. The highest Cr (VI) removal yields of 48.2, 30.8 and 30.5% were achieved at pH=2 and particle size 0.355 mm using OPB-Al<sub>2</sub>O<sub>3</sub>, CC-Al<sub>2</sub>O<sub>3</sub> and OP-Al<sub>2</sub>O<sub>3</sub>, respectively. For mercury ions, the highest removal yields were obtained at pH=6 (70.89, 34.18 and 54.9 % using OPB-Al<sub>2</sub>O<sub>3</sub>, CC-Al<sub>2</sub>O<sub>3</sub> and OP-Al<sub>2</sub>O<sub>3</sub>, respectively). These results are attributed to induced changes in biosorbent surface that increases the adsorption of metal ions such as mercury that is predominantly present in Hg (OH)<sup>2+</sup> and HgCl<sup>2+</sup> forms, producing electrostatic attraction with OH<sup>-</sup> anions at higher pH<sup>33</sup>. On the other hand, protonation in acid solution induces an electrostatic repulsion that reduces the number of active sites available for the adsorption of mercury ions. Many researchers have obtained similar results<sup>34</sup> reported that Hg (II) is better adsorbed at pH ranged in 4-6. The competition for available adsorption sites of H<sup>+</sup> with cationic forms of mercury at pH>4 is lower than acid pH<sup>35</sup> evaluated the effect of pH (1-12) on Hg (II) removal onto a hyperbranched and multi-functionalized dendrimer modified mixed-oxides nanoparticles, finding that the highest removal yield (99.9%) was reached at pH=6 and pH>9 induces precipitation of this metal.

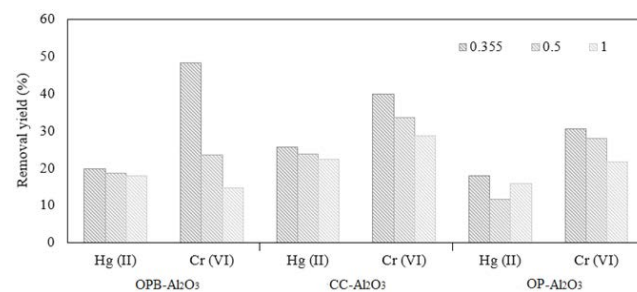


**Figure 4.** Effect of particle size on the removal yield of Cr (VI) and Hg (II) using biomaterials modified with Al<sub>2</sub>O<sub>3</sub> nanoparticles at pH=2.

**Adsorption equilibrium time:** Figures 7 and 8 show the contact time overtime required to reach the equilibrium in the system biosorbent-heavy metal ions for Cr (VI) and Hg (II). After this time adsorption process started to be stable indicating saturation of active sites due to the

repulsive forces between cations already set and the free ones in solution affect rate of adsorption overtime<sup>36</sup>. This experiments were carried out at suitable conditions of pH and particle size. The adsorption equilibrium time ranged between 350-390 min and 270-330 min for chromium and mercury, respectively. It was found that Hg (VI) saturated the biosorbents more quickly than Cr (VI), which can be attributed to the high availability of active sites offered at pH=6<sup>16</sup>.

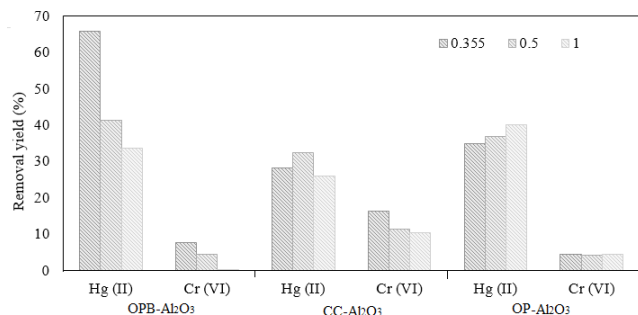


**Figure 5.** Effect of particle size on the removal yield of Cr (VI) and Hg (II) using biomaterials modified with  $\text{Al}_2\text{O}_3$  nanoparticles at pH=4.

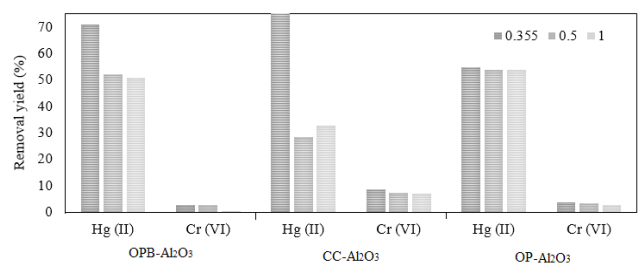


**Figure 6.** Effect of particle size on the removal yield of Cr (VI) and Hg (II) using biomaterials modified with  $\text{Al}_2\text{O}_3$  nanoparticles at pH=6.

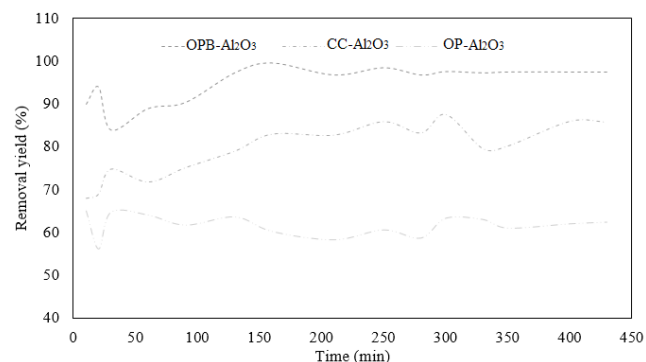


**Figure 7.** Hg (II) adsorption equilibrium time using biomaterials modified with  $\text{Al}_2\text{O}_3$  nanoparticles at pH=6.

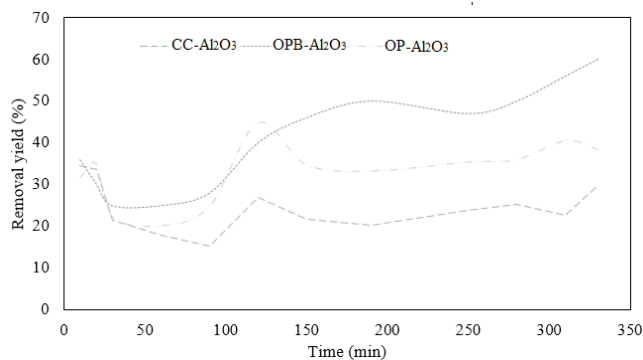


**Figure 8.** Cr (VI) adsorption equilibrium time using biomaterials modified with  $\text{Al}_2\text{O}_3$  nanoparticles at pH=2.

## 4. Conclusions

This work studied the adsorption of Cr (VI) and Hg (II) ions onto residual biomass (orange peels, oil palm bagasse and corn cob) modified with  $\text{Al}_2\text{O}_3$  nanoparticles. It was found that pH most affects removal yield of both heavy metals. The suitable conditions for carrying out further experiments were pH=2 and 6 for Cr (VI) and Hg (II), respectively. In addition, particle size did not significantly affect adsorption process, however the highest removal yields were reached at 0.355 mm. For Hg (II) ions, the highest removal yields were 70.89, 34.18 and 54.9 % using OPB- $\text{Al}_2\text{O}_3$ , CC- $\text{Al}_2\text{O}_3$  and OP- $\text{Al}_2\text{O}_3$ , respectively. For Cr (VI) ions, these values were 48.2, 39.8 and 30.5 % using OPB- $\text{Al}_2\text{O}_3$ , CC- $\text{Al}_2\text{O}_3$  and OP- $\text{Al}_2\text{O}_3$ , respectively. According to these results, OPB- $\text{Al}_2\text{O}_3$  is recommended as biosorbent in Hg (II) and Cr (VI) uptake applications due to its efficiency and availability of low-cost raw material.

## 5. Acknowledgments

The authors are thankful to COLCIENCIAS and University of Cartagena for their support to carry out this study.

## 6. References

1. Imam SSA, Rajpoot IK, Gajjar B, Sachdeva A. Comparative study of heavy metal bioremediation in soil by bacillus subtilis and saccharomyces cerevisiae. Indian Journal of Science and Technology. 2016; 9(47):1-7.
2. Mehta K. Impact of temperature on contaminants toxicity in fish fauna: A review. Indian Journal of Science and Technology. 2017; 10(18):1-6. Crossref

3. Tejada-Tovar C, Villabona-Ortíz A, Herrera-Barros A, González-Delgado AD, Garcés L. Adsorption kinetics of Cr (VI) using modified residual biomass in batch and continuous system. *Indian Journal of Science and Technology*. 2018; 11(14):1–8. Crossref
4. Gibb H, O'Leary KG. Mercury exposure and health impacts among individuals in the artisanal and small-scale gold mining community: A comprehensive review. *Environmental Health Perspective*. 2014; 122:667–72. Crossref
5. Liu Z, Li-ao W, Xu J, Ding S, Feng X, Xiao H. Effects of different concentrations of mercury on accumulation of mercury by five plant species. *Ecological Engineering*. 2017; 106:273–8. Crossref
6. Tejada-Tovar C, Gonzalez-Delgado AD, Villabona-Ortiz A. Removal of Cr (VI) from aqueous solution using orange peel-based biosorbents. *Indian Journal of Science and Technology*. 2018; 11(13):1–13. Crossref
7. Zhao L, Huang Y, Chen H, Zhao Y, Xiao T. Study on the preparation of bimetallic oxide sorbent for mercury removal. *Fuel*. 2017; 197:20–7. Crossref
8. Tejada-Tovar C, Montiel Z, Acevedo D. Aprovechamiento de cáscaras de yuca y -ame para el tratamiento de aguas residuales contaminadas con Pb (II). *Información Tecnológica*. 2016; 27(1):9–20. Crossref
9. Gogoi S, Chakraborty S, Saikia MD. Surface modified pineapple crown leaf for adsorption of Cr(VI) and Cr(III) ions from aqueous solution. *Journal of Environmental Chemical Engineering*. 2018; 6(2):2492–501. Crossref
10. El-Zawahry M, Abdelghaffar F, Abdelghaffar RA, Hassabo A. Equilibrium and kinetic models on the adsorption of Reactive Black 5 from aqueous solution using Eichhorniacrassipes/chitosan composite. *Carbohydrate Polymers*. 2016; 136:507–15. Crossref PMID:26572382
11. Rawtani D, Khatri N, Tyagi S, Pandey G. Nanotechnology-based recent approaches for sensing and remediation of pesticides. *Journal of Environmental Management*. 2018; 206:749–62. Crossref PMID:29161677
12. Ghaedi M, Mosallanejad N. Study of competitive adsorption of malachite green and sunset yellow dyes on cadmium hydroxide nanowires loaded on activated carbon. *Journal of Industrial and Engineering Chemistry*. 2014; 20:1085–96. Crossref
13. Behnajady MA, Bimeghdar S. Synthesis of mesoporous NiO nanoparticles and their application in the adsorption of Cr(VI). *Chemical Engineering Journal*. 2014; 239:105–13. Crossref
14. Mohammadi A, Daemi H, Barikani M. Fast removal of malachite green dye using novel superparamagnetic sodium alginate-coated Fe<sub>3</sub>O<sub>4</sub> nanoparticles. *International Journal of Biological Macromolecules*. 2014; 69:447–55. Crossref PMID:24875322
15. Santosh C, Velmurugan V, Jacob G, Jeong SK, Grace AN, Bhatnagar A. Role of nanomaterials in water treatment applications: A review. *Chemical Engineering Journal*. 2016; 306:1116–37. Crossref
16. Tejada-Tovar C, Herrera A, Ruiz E. Kinetic and isotherms of biosorption of Hg(II) using citric acid treated residual materials. *Ingeniería y competitividad*. 2016; 18(1):117–27.
17. Tejada-Tovar C, Villabona-Ortíz A, Ruiz E. Adsorción de Ni (II) por cáscaras de -ame (*Dioscorea rotundata*) y bagazo de palma (*Elaeis guineensis*) pretratadas. *Revista Luna Azul*. 2016; 42:30–43.
18. Tejada-Tovar C, Herrera A, Núñez J. Adsorción competitiva de Ni (II) y Pb(II) sobre materiales lignocelulósicos. *Investigaciones Andina*. 2015; 17(31):1354–67.
19. Naik K, Moitra D, Dayananda D. A facile method for preparation of TiO<sub>2</sub> nanoparticle loaded mesoporous  $\gamma$ -Al<sub>2</sub>O<sub>3</sub>: An efficient but cost-effective catalyst for dye degradation. *Journal of Nanoscience and Nanotechnology*. 2016; 16(8):8544–9. Crossref
20. Rejaeiyan A, Bagheri-Mohagheghi MM. Comparison of sol-gel and co-precipitation methods on the structural properties and phase transformation of  $\gamma$  and  $\alpha$ -Al<sub>2</sub>O<sub>3</sub> nanoparticles. *Advances in Manufacturing*. 2013; 1(2):176–82. Crossref
21. Mohseni M, Gilani K, Mortazavi SA. Preparation and characterization of rifampin loaded mesoporous silica nanoparticles as a potential system for pulmonary drug delivery. *Iranian Journal of Pharmaceutical Research*. 2015; 14(1):27–34. PMID:25561909 PMCid:PMC4277616
22. Sadri M, Pedbeni A, Hossein H. Preparation of biopolymeric nanofiber containing silica and antibiotic. *Journal of nanostructures*. 2016; 6(1):93–7.
23. Tejada-Tovar C, Villabona-Ortiz A, Ruiz E. Cinética de adsorción de Cr (VI) usando biomazas residuales modificadas químicamente en sistemas por lotes y continuo. *Revista Ion*. 2015; 28(1):29–41.
24. Zapata-Acosta K, Piedrahita AM, Alzate AF, Cortés FB, Rojano B. Oxidative Stabilization of Sacha Inchi (*Plukenetia volubilis* Linneo) Oil with Morti-o (*Vaccinium meridionale* SW) Suspensions Addition. *Revista Ciencia en Desarrollo*. 2015; 6(2):141–53.
25. Doria-Herrera G, Paz-Ordoñez M, Hormanza-Anaguano A. Estandarización de la difenilcarbazida como indicador y acomplejante en la identificación de cromo hexavalente- Cr (VI). *Producción + Limpia*. 2013; 8(2):9–20.
26. Longa J, Yu X, Xu E. In situ synthesis of new magnetite chitosan/carrageenan nanocomposites by electrostatic interactions for protein delivery applications. *Carbohydrate Polymers*. 2015; 131:98–107. Crossref PMID:26256165
27. Leyva-Ramos R, Landin-Rodríguez LE, Leyva-Ramos S, Medellín-Castillo N. Modification of corncob with citric

- acid to enhance its capacity for adsorbing cadmium (II) from water solution. *Chemical Engineering Journal*. 2012; 180:113–20. Crossref
28. Nazari M, Halladj R. Adsorptive removal of fluoride ions from aqueous solution by using sonochemically synthesized nanomagnesia/alumina adsorbents: An experimental and modeling study. *Journal of the Taiwan Institute of Chemical Engineers*. 2014; 45(5):2518–25. Crossref
  29. Amirsalari A, Farjami-Shayesteh S. Effects of pH and calcination temperature on structural and optical properties of alumina nanoparticles. *Superlattices and Microstructures*. 2015; 82:507–24. Crossref
  30. Tejada-Tovar C, Villabona-Ortíz A, Garcés-Jaraba L. Adsorption of heavy metals in waste water using biological materials. *Tecno Lógicas*. 2015; 18(34):109–23. Crossref
  31. Tejada-Tovar, Herrera A, Zarur J. Remoción de plomo por biomasa residual de cáscara de naranja (*Citrus sinensis*) y zuro de maíz (*Zea Mays*). *Revista U.D.C.A Actualidad and Divulgación Científica*. 2016; 19(1):169–78.
  32. Gupta A, Balomajumder C. Simultaneous removal of Cr(VI) and phenol from binary solution using *Bacillus* sp immobilized onto tea waste biomass. *Journal of Water Process Engineering*. 2015, 6, pp. 1-10. Crossref
  33. Fakhri A. Investigation of mercury (II) adsorption from aqueous solution onto copper oxide nanoparticles: Optimization using response surface methodology. *Process Safety and Environmental Protection*. 2015; 93:1–8. Crossref
  34. Oveisi F, Nikazar M, Hossein-Razzaghi M, Taghi JM, Al-Sadat M. Effective removal of mercury from aqueous solution using thiol-functionalized magnetic nanoparticles. *Environmental Nanotechnology, Monitoring and Management*. 2017; 7:130–8. Crossref
  35. Arshadi M, Mousavinia F, Khalafi-Nezhad A, Firouzabadi H, Abbaspourrad A. Adsorption of mercury ions from wastewater by a hyperbranched and multi-functionalized dendrimer modified mixed-oxides nanoparticles. *Journal of Colloid and Interface Science*. 2017; 505:293–306. Crossref PMID:28582722
  36. Ben-Ali S, Jaouali I, Souissi-Najar S, Ouederni A. Characterization and adsorption capacity of raw pomegranate peel biosorbent for copper removal. *Journal of Cleaner Production*. 2017; 144:553–8. Crossref